# A superposed epoch analysis of auroral evolution during substorms: Local time of onset region

S. E. Milan,[1] A. Grocott,[1] and B. Hubert[2]

Received 11 May 2010; revised 6 June 2010; accepted 21 July 2010; published 14 October 2010.

[1] Previous workers have shown that the magnetic local time (MLT) of substorm onset depends on the prevailing east-west component of the interplanetary magnetic field (IMF). To investigate the influence of the onset MLT on the subsequent auroral response we perform a superposed epoch analysis of the auroral evolution during approximately 2000 substorms using observations from the FUV instrument on the Imager for Magnetopause-to-Aurora Global Exploration (IMAGE) spacecraft. We subdivide the substorms by onset latitude and onset local time before determining average auroral images before and after substorm onset, for both electron and proton aurorae. We find that during the growth phase there is preexisting auroral emission in the MLT sector of the subsequent onset. After onset the auroral bulge expands eastward and westward, but remains centered on the onset sector. Approximately 30 min after onset, during the substorm recovery phase, the peaks in electron and proton auroral emission move into the postnoon and prenoon sectors, respectively, reflecting the "average" auroral precipitation patterns determined by previous studies. Superposed epoch analysis of the interplanetary magnetic field for the substorms under study suggests that the $B_Y$ component of the IMF must be biased toward positive or negative values for up to a day prior to onset for the onset MLT to be influenced.

**Citation:** Milan, S. E., A. Grocott, and B. Hubert (2010), A superposed epoch analysis of auroral evolution during substorms: Local time of onset region, *J. Geophys. Res.*, *115*, A00I04, doi:10.1029/2010JA015663.

## 1. Introduction

[2] As the magnetosphere accumulates open magnetic flux through the action of magnetic reconnection near the subsolar point [e.g., *Dungey*, 1961, 1963] the magnetotail inflates and the stress imposed on the tail magnetopause by the flow of the solar wind increases. Eventually, a substorm is triggered to release open magnetic flux back to the solar wind by reconnection in the neutral sheet of the tail. This two stage process has been described as the loading/unloading cycle [e.g., *Baker et al.*, 1996] or equivalently the expanding/contracting polar cap paradigm (ECPC) [e.g., *Cowley and Lockwood*, 1992; *Lockwood and Cowley*, 1992; *Milan et al.*, 2003, 2007, 2008], and is responsible for the circulation of plasma within the magnetosphere known as the Dungey cycle. The substorm process, as a global reconfiguration of magnetospheric state, manifests itself in many observables including the magnetic field and plasma distributions within the magnetotail, and electric currents and plasma convection in the ionosphere. The most visible manifestation is the auroral evolution associated with the substorm cycle; observationally, a global picture of the evolution can be gained from either a synthesis of many ground-based observations [e.g., *Akasofu*, 1964] or using satellite-borne cameras to gain global snapshots of the auroral distribution [e.g., *Frank and Craven*, 1988; *Mende et al.*, 2003]. In recent years, auroral imaging missions have gathered sufficient observations to allow a statistical investigation of the global auroral dynamics related with substorms. For instance, *Mende et al.* [2003] performed a superposed epoch analysis of 91 substorms observed using the Imager for Magnetopause-to-Aurora Global Exploration (IMAGE) spacecraft, showing equatorward expansions and poleward contractions of the auroral oval prior to and after substorm onset, consistent with the ECPC, and an offset between the locations of electron and proton aurorae consistent with the expected locations of the region 1 and 2 current systems. Subsequently, *Frey et al.* [2004] employed 2 years of observations to identify the onset times and locations of over 2000 substorms.

[3] More recently, *Milan et al.* [2009a] conducted a superposed epoch analysis of the auroral activity during the 2000 substorms identified by *Frey et al.* [2004] to investigate the unloading response to differing amounts of open flux in the magnetosphere at the time of substorm onset, estimated from the latitude of the substorm onset. That study concluded that the unloading process was more intense if a larger amount of open flux had been accumulated prior to onset, manifested by a greater contraction of the polar cap during the expansion phase of the substorm and a brighter

[1]Department of Physics and Astronomy, University of Leicester, Leicester, UK.
[2]Laboratory of Planetary and Atmospheric Physics, University of Liege, Liege, Belgium.


0148-0227/10/2010JA015663

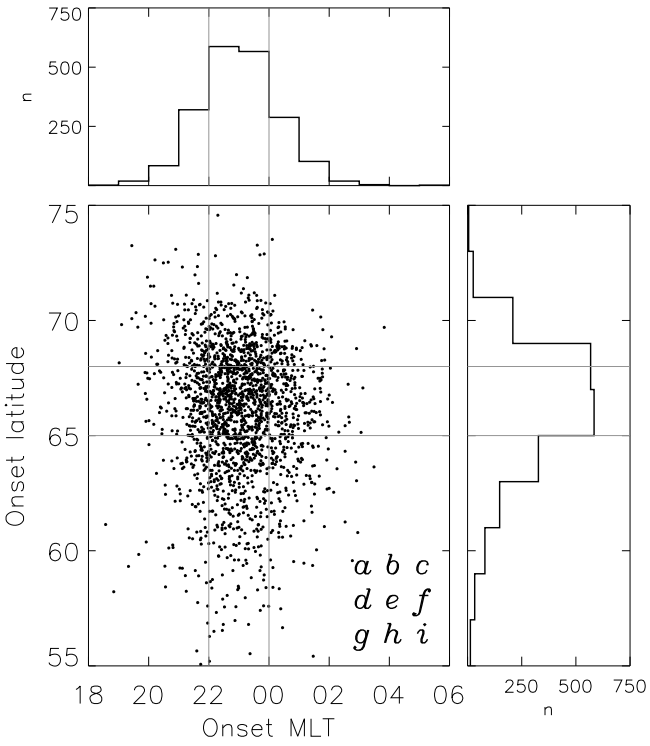


**Figure 1.** The distribution of magnetic local time and magnetic latitude of onset of the approximately 2000 substorms taken from the list of *Frey et al.* [2004] used in this study. The onsets have been subdivided into 9 categories by latitude and MLT as indicated by the horizontal and vertical gray lines. These categories have been labeled *a* to *i* as indicated in the letters in the bottom right of Figure 1 (bottom left).

substorm auroral bulge. *Milan et al.* [2009a] speculated that the electrodynamics of the substorm process could depend systematically on onset latitude, modified by the ionospheric conductivity within the auroral bulge, and this was subsequently confirmed by *Grocott et al.* [2009] who demonstrated the expected differences in the ionospheric convection response to substorms. A key finding of *Milan et al.* [2009a] was that substorm onset latitude is at least partly determined by the intensity of the ring current, suggesting that the magnetic perturbation associated with an enhanced ring current can stabilize the magnetotail to reconnection, increasing the amount of open flux that can be sustained before onset is triggered. This ring current influence on substorm onset latitude was further investigated by *Milan et al.* [2009b] and *Milan* [2009].

[4] This still leaves open questions regarding the exact nature of the substorm onset mechanism. In particular, this does not explain the observed distribution of magnetic local times (MLTs) of onset. Previous studies of onset MLT, including those of *Mende et al.* [2003], *Gérard et al.* [2004] and *Frey et al.* [2004], have found that substorms tend to brighten initially in the premidnight sector, near 23 MLT, though onsets can occur between 20 and 02 MLT. *Østgaard et al.* [2005, 2007] examined the dependence of the onset MLT on the prevailing east–west or $B_Y$ component of the interplanetary magnetic field (IMF) and found indeed that onsets occurred at earlier and later MLTs (in the northern hemisphere) for $B_Y > 0$ nT and $B_Y < 0$ nT. In this study we investigate the influence of the MLT of onset on the development of the substorm. We perform a superposed epoch analysis of the auroral development, similar to that performed by *Milan et al.* [2009a], with substorms categorized by both onset latitude and MLT. In this way, we examine the auroral behavior both prior to and after substorm onset and discuss the ramifications for substorm processes.

## 2. Methodology

[5] The methodology of the present study follows closely that of *Milan et al.* [2009a] in which superposed epoch analyses of auroral evolution during substorms were undertaken. We use the substorm onset list of *Frey et al.* [2004], which includes approximately 2000 substorms identified in IMAGE satellite observations of the northern hemisphere UV aurorae between June 2000 and May 2002, inclusive. Observations were made by the Far Ultraviolet (FUV) instrument [*Mende et al.*, 2000a, 2000b] which included the Wideband Imaging Camera (WIC) and the Spectrographic Imager (SI12). WIC was sensitive to auroral emissions over a broad range of the UV spectrum, 1200 to 2000 Å, the primary component of which is produced by precipitating electrons and associated secondaries, although proton precipitation can also contribute by secondary electron production. SI12 imaged Doppler-shifted Lyman $\alpha$ emission associated with precipitating protons. *Frey et al.* [2004] identified the onset time, the magnetic latitude of onset, and the onset MLT of each substorm. Figure 1 shows the distribution of the onsets in MLT and latitude. Most onsets occur in the 22 to 24 MLT sector, which we will refer to as the "typical" onset region. Most other onsets occur in the 20 to 22 MLT and 00 to 02 MLT sectors, which we will refer to as "early" and "late" onsets. For the purposes of averaging we subdivide the onsets into 9 categories by latitude and MLT, indicated by the vertical and horizontal gray lines in Figure 1. We have designated these categories by the letters *a* to *i*, as indicated by the letters in the bottom right-hand corner of Figure 1. The original study of *Milan et al.* [2009a] divided the substorms into 5 onset latitude bands; here we use just 3 latitude bands to maintain a statistically significant number of substorms in each category when we further subdivide by onset MLT.

[6] Within each category we produce superposed epoch analyses of the auroral evolution keyed to substorm onset time, for both WIC and SI12. Average auroral images are produced for 10 min intervals from 1 h prior to 2 h after onset. For each such average image we determine the maximum auroral brightness in 48 MLT bins, each 0.5 h wide. The results are shown in Figure 2 for SI12 (HI Lyman-$\alpha$, predominantly protons) and Figure 3 for WIC (NI atomic lines and N2 LBH, predominantly electrons). In Figures 2 and 3 there are 9 panels corresponding to the 9 categories identified in Figure 1. Each panel represents the evolution of the local time distribution of brightness in the auroral zone (horizontally) as a function of time during the average substorm (vertically). In each panel, a vertical dashed line indicates local midnight and a horizontal dashed line indicates substorm onset. A slightly different color scale is used in each latitude band as *Milan et al.* [2009a] showed

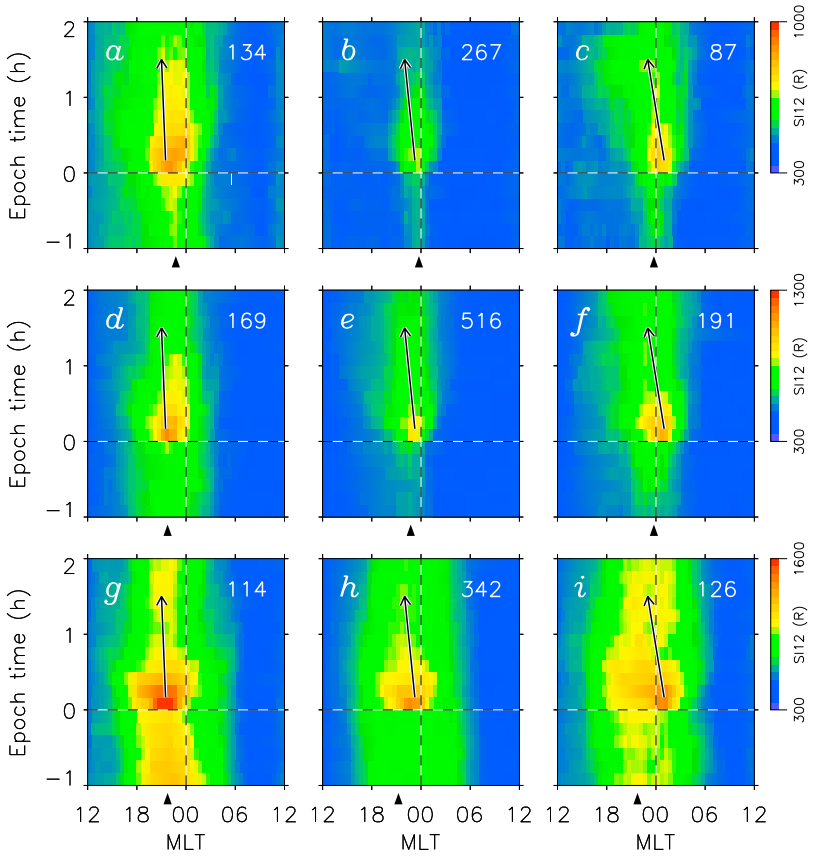


**Figure 2.** Superposed epoch analyses of the evolution of the magnetic local time distribution of SI12 auroral brightness during substorms, from 1 h before to 2 h after onset. (a–i) The plots correspond to the 9 magnetic latitude and MLT categories identified in Figure 1. Horizontal lines show the time of onset and vertical lines the local midnight meridian. Numbers in the top right of each plot show the number of substorms that contributed to each analysis. The color scales are linear. Arrows indicate the main direction of evolution of the centroid of auroral brightness following onset.

that the auroral intensity increases with decreasing latitude of onset.

[7] In the case of Figure 3 and the WIC observations there are no observations between 07 and 17 MLT as this part of the oval is obscured by dayglow. To further reduce the detrimental effects of dayglow, we have limited the WIC observations to the five months centered on winter solstice. Numbers in the top right of each panel of Figures 2 and 3 show the number of substorms that contributed toward the SI12 and WIC analyses in each category.

[8] We also investigate the interplanetary magnetic field (IMF) and solar wind precursors of the early, typical, and late category substorms, and the geomagnetic response to these substorms, by performing superposed epoch analyses of IMF $B_Y$ and $B_Z$, solar wind speed and density, $V_{SW}$ and $N_{SW}$, the electroject indices AU and AL, and the ring current index Sym-H, as presented in Figures 4 and 5. Solar wind plasma and magnetic field measurements are taken from the Solar Wind Electron, Proton, and Alpha Monitor (SWEPAM) and Magnetic Fields Experiment (MFE) instruments [*McComas et al.*, 1998; *Smith et al.*, 1998] onboard the Advanced Composition Explorer (ACE) spacecraft [*Stone et al.*, 1998]. Solar wind and IMF observations are propagated from the position of ACE to the magnetopause by considering the solar wind velocity. The thick lines of Figures 4 and 5 show the median variations, with the upper and lower curves showing the quartiles. We combine all the onset latitude bands together to examine solely the influence of the onset MLT; similar superposed epoch analyses of these parameters ordered by onset latitude can be found from the work of *Milan et al.* [2009a].

## 3. Observations

[9] Figures 2 and 3 present superposed epoch analyses of the evolution of the local time distribution of auroral brightness during substorms, categorized by onset latitude and magnetic local time. In each case there is a clear enhancement in auroral brightness at the zero epoch time, as expected. Moreover, the location of the initial brightening is at earlier MLTs in the left-hand columns (the early onsets) and later MLTs in the right hand columns (the late onsets). This gives confidence in the selection criteria of *Frey et al.* [2004] that we have used to categorize the substorms.

[10] There is a clear dependence on the onset MLT of the auroral brightness of the substorms, those occurring in the typical onset sector being dimmer than early and late onsets. This is confirmed in Figure 6, which shows the peak post-onset brightness for each category in (a) SI12 and (b) WIC. For both SI12 and WIC there is an overall increase in

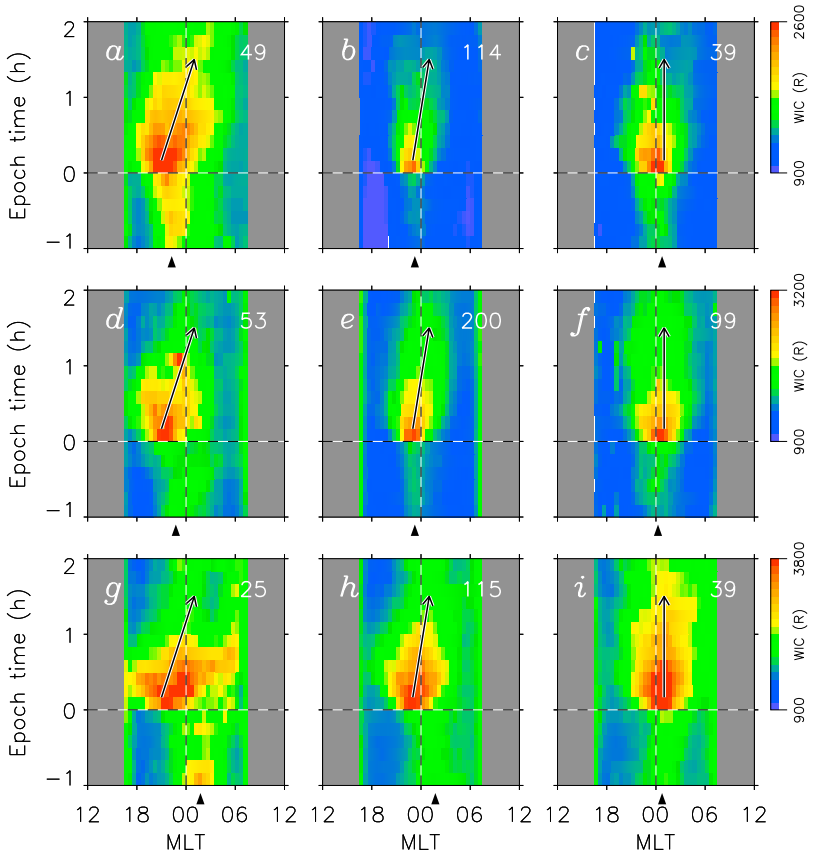


**Figure 3.** Similar to Figure 3 for WIC. Local times from 07 to 17 MLT are obscured due to the contribution of dayglow.

brightness for low latitude onsets as previously reported by *Milan et al.* [2009a]; in addition to this overall trend, there is a clear minimum in peak postonset brightness for typical substorms.

[11] Following the initial brightening at zero epoch time, the auroral bulge spreads to earlier and later local times for up to 30 min after onset, typically to a width of 6 h of local time. In most cases this expansion occurs roughly symmetrically about the onset MLT, such that the center of the auroral bulge remains in the onset sector. After about 30 min the bulge begins to dim, though can remain brighter than preonset levels for up to 2 h after onset. During this fading – or recovery – phase the centroid of SI12 auroral emission moves to the premidnight sector whereas the centroid of WIC emission moves toward the postmidnight sector. This auroral configuration reflects the average locations of proton and electron auroral activity, as previously reported by *Milan et al.* [2009a, 2010].

[12] Of particular interest is the auroral configuration prior to onset. For low-latitude onsets (categories *g*, *h*, and *i*) there is considerable preexisting auroral emission premidnight for SI12 and postmidnight for WIC: this reflects the average locations of proton and electron aurorae during the recovery phase as described above, suggesting that low-latitude substorms occur during intervals when there is almost continuous auroral activity from one substorm to the next. For higher latitude, less energetic substorms (categories *a* to *f*) there is also preexisting emission within the oval. Crucially, this preexisting emission tends to be brightest in the local time sector in which the onset is subsequently observed. For each category of substorm we have determined the centroid of emission in the hour prior to onset, indicated by arrows at the bottom of each of the panels in Figures 2 and 3. For both SI12 and WIC, the location of this centroid occurs at earlier and later local times for early and late onsets. This is presented in another format in Figure 7. Here the MLT of the centroid in preonset emission is indicated for the 9 onset categories for both (a) SI12 and (b) WIC. As described above, the preonset emission associated with low-latitude substorms peaks in the premidnight and postmidnight sectors for SI12 and WIC, respectively. For higher latitude substorms the preonset emission is observed close to 23 MLT for typical onsets and moves to earlier and later local times for early and late onsets.

[13] The growth, expansion, and recovery phase auroral observations described above are summarized schematically in Figure 8. The intensity of electron and proton aurorae are indicated by gray scale and line contours, respectively. Early and late onset substorms are indicated to the left and right of Figure 8. In the case of low-latitude onsets the growth phase auroral configuration shown in Figure 8 is on average obscured by recovery phase auroral luminosity from the preceding substorm.

[14] Figure 4 presents superposed epoch analyses of solar wind, IMF, and geomagnetic indices keyed to onset time. The IMF $B_Z$ variation shows a southward turning of the IMF up to 2 h prior to onset, with a recovery to less negative $B_Z$

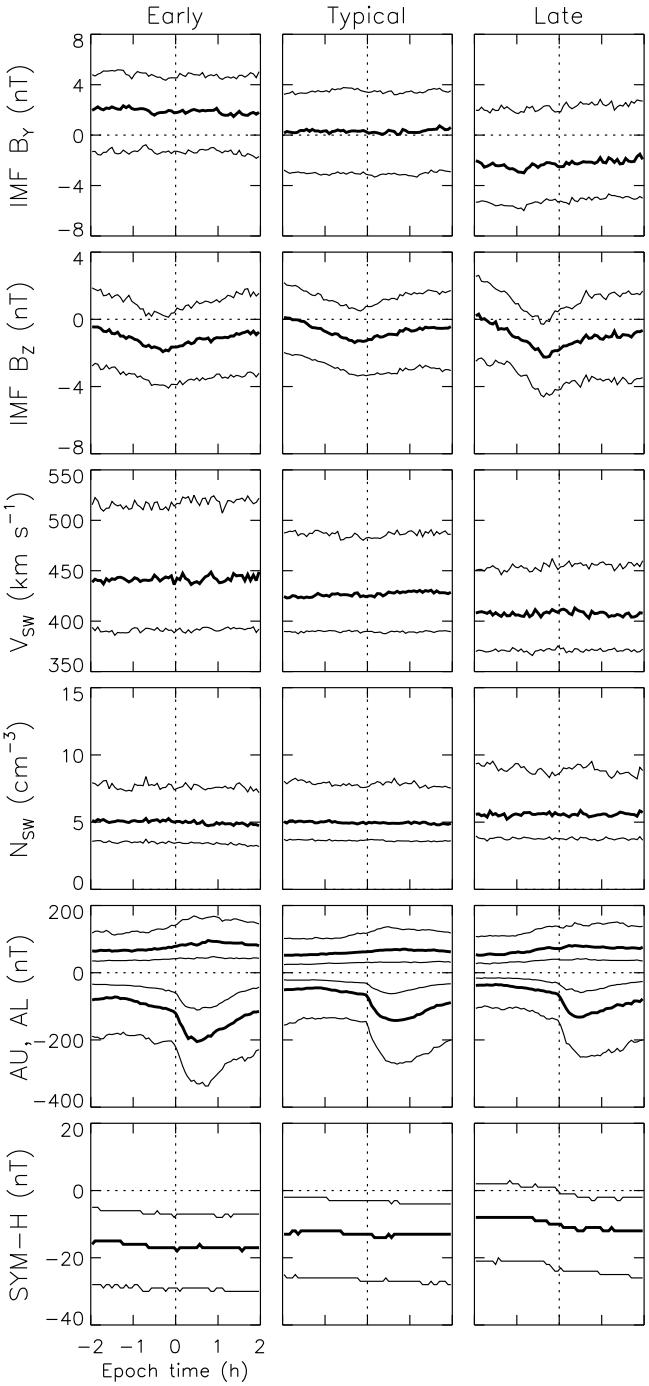


**Figure 4.** Superposed epoch analyses of solar wind, interplanetary magnetic field, and geomagnetic activity from 2 h before to 2 h after onset, for all early, typical, and late onsets. Thick lines indicate the median variation, thin lines the quartiles.

after onset. The early and late onsets are associated with slightly more negative $B_Z$ than typical onsets. The most significant difference between the onset categories is the tendency for IMF $B_Y$ to be positive during early onsets and negative during late onsets, with no bias for typical onsets; these observations are consistent with the findings of *Østgaard et al.* [2005, 2007]. *Østgaard et al.* [2005, 2007] furthermore showed that the sense of the shift in local time of onset with $B_Y$ was opposite in the northern and southern hemispheres. There is a progressive decrease in solar wind velocity with the MLT of onset from early to late onset; solar wind density is largely independent of onset MLT. AU and AL show typical substorm signatures, though the AL signature is progressively less negative the later the MLT of onset. Averaged over all substorms, the Sym-H index shows quiet time values.

[15] To examine the IMF dependence of onsets in more detail, Figure 5 presents superposed epoch analyses of $B_Y$ and $B_Z$ over a longer time period, from 40 h before to 20 h after onset. The $B_Z$ traces emphasize the 1 to 2 h duration of the southward turning prior to onset; after onset the tendency to southward IMF decreases over the next 5 or so hours. The $B_Y$ traces indicate that the tendency to positive and negative $B_Y$ prior to early and late onsets becomes significant up to a day prior to the substorm; this bias decreases over the 10 or so hours after onset.

## 4. Discussion

[16] Superposed epoch analyses of auroral imagery and upstream solar wind measurements show that the local time of the auroral onset depends on the prevailing east–west component of the interplanetary magnetic field. The IMF must turn southward for 1 to 2 h prior to onset to increase the open magnetic flux content of the magnetosphere, the substorm growth phase, before onset is triggered. After onset the median $B_Z$ becomes less negative as southward IMF is no longer necessary to precipitate the substorm and the IMF has a tendency to change its north–south polarity on a timescale of 10s of minutes [e.g., *Freeman and Morley*, 2009]. In contrast to the 1 to 2 h growth phase, the $B_Y$ component shows a bias toward positive or negative values up to a day before early and late onsets, respectively. This bias reduces after onset, in much the same way as the negative $B_Z$, as it is no longer necessary and the IMF is naturally changeable. The timescale for the relaxation of $B_Y$ is longer than that of $B_Z$, indicating that $B_Z$ is more variable than $B_Y$, as can be verified by comparing the autocorrelation functions of these two components, presented in Figure 9. If the MLT of substorm onset was determined by the sense of $B_Y$ just at the time of onset we would expect the rise and fall of $|B_Y|$ prior to and after onset to be symmetrical. However, the rise in $|B_Y|$ before onset has a longer duration than the fall, suggesting that $B_Y$ must be positive or negative for several hours prior to onset to influence the onset category. If the onset MLT is determined by a twist induced in the magnetotail by a predominance of magnetotail lobe field lines opened under one sense of $B_Y$ or another [e.g., *Cowley*, 1981], then this $B_Y$ may have to prevail for a significant period of time. For instance, if substorms are typically associated with the opening and subsequent closure of a third of the open flux in the magnetosphere [e.g., *Milan et al.*, 2007], then for one sense of $B_Y$ to dominate in the magnetotail it must have persisted in the solar wind for the previous 2 to 3 growth phases.

[17] Figure 4 suggests that early and late substorms are on average associated with brighter expansion phase emission

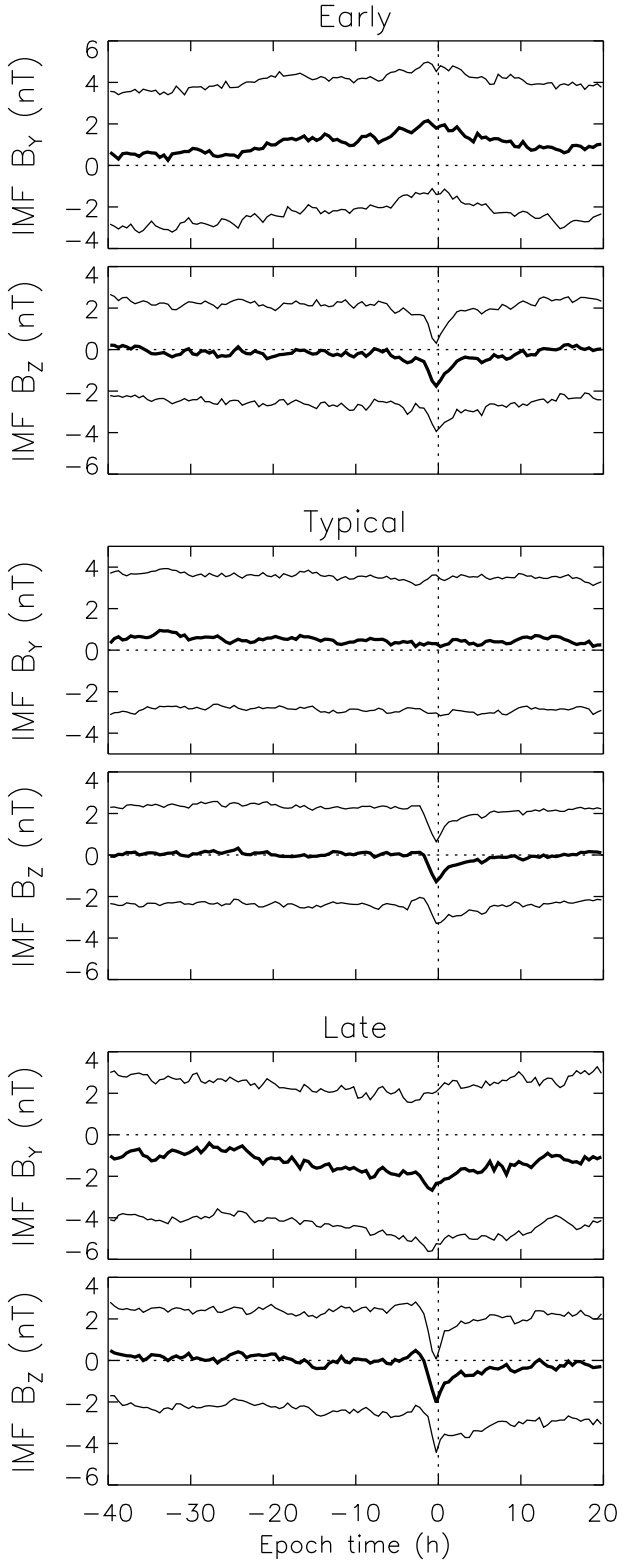


**Figure 5.** Superposed epoch analyses of IMF $B_Y$ and $B_Z$ for all early, typical, and late substorms, from 40 h before to 20 h after onset. Thick lines indicate the median variation, thin lines the quartiles.

than typical substorms. We note that the growth phase IMF $B_Z$ for nontypical substorms is more negative than in the typical case (Figure 6), indicating that this enhanced auroral activity is probably caused by a greater level solar wind-magnetosphere coupling during these events.

[18] Once onset occurs the auroral signature of the brightening bulge expands eastward and westward, relatively symmetrically about the onset location in most categories. *Liou et al.* [2006] reported that a detailed analysis of the expansion velocities to the east and west reveal a $B_Y$-related asymmetry, but the local time binning of our observations is too coarse to verify this. Approximately 30 min after onset the centroids of the proton and electron emission begin to move into the premidnight and postmidnight sectors, respectively, irrespective of the original onset location. This latter pattern matches the "average" electron and proton precipitation configurations identified in IMAGE observations by, among others, *Milan et al.* [2009a, 2010], also consistent with the average pattern of electron and ion precipitation observed with DMSP satellites by *Hardy et al.* [1985, 1989] and *Gussenhoven et al.* [1987]. As discussed by *Gussenhoven et al.* [1987], the asymmetry in shape and intensity is associated with the directions that protons and electrons drift around the Earth after being injected into the inner magnetosphere from the magnetotail. Hence, we see the evolution of the auroral configuration from (a) the initial breakup region, where precipitation is driven by processes in the magnetotail associated with substorm onset, to (b) the spreading of the bulge which is a tracer of the magnetotail reconfiguration associated with substorm expansion phase, to (c) the recovery phase auroral pattern associated with injected particles trapped in the inner magnetosphere and drifting dawnward and duskward.

[19] Low-latitude onsets have growth phase auroral emission in the location expected for the recovery phase of the preceding substorm, that is proton (electron) auroral emission maximizing in the premidnight (postmidnight) sector. This relatively bright emission associated with the inner magnetosphere will mask fainter emission associated with growth phase dynamics of the tail. Higher latitude onsets, however, have a growth phase auroral configuration that presages the onset location of the following expansion phase. There is a peak in auroral brightness in the approximate local time sector in which the onset subsequently occurs, determined by the prevailing sense of IMF $B_Y$ as discussed above. Here we discuss a few mechanisms that could lead to a peak in emission in the onset region prior to onset.

[20] One possibility is that the region of the magnetotail in which onset subsequently occurs moves to earlier and later local times for positive and negative IMF $B_Y$. This is inconsistent with the observation of *Østgaard et al.* [2005, 2007] that the onset MLT moves in opposite senses in the northern and southern hemispheres for a given $B_Y$ polarity in the IMF, and we expect the onset to be magnetically conjugate in the two hemispheres. Rather, we favor the interpretation that the magnetotail is twisted by a preponderance of lobe field lines connected to one sense of IMF $B_Y$ or the other [*Cowley*, 1981]. This leads to mapping of an approximately centrally located onset region into the premidnight and postmidnight ionospheres in the northern and

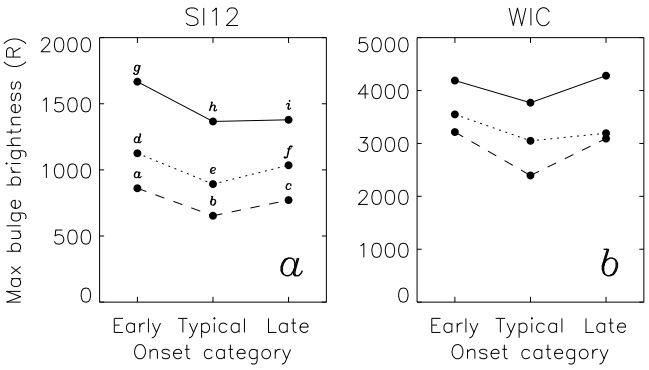


**Figure 6.** The peak emission brightness during the expansion phase of substorms in the categories *a* to *i* for (a) SI12 and (b) WIC. The letters associated with the categories are indicated in Figure 6a. Solid, dotted, and dashed curves correspond to the low, middle, and high onset latitude categories, respectively.

southern hemispheres for positive $B_Y$ and vice versa for negative $B_Y$. Activity in this central region of the tail, leading to auroral emission during the growth phase in the magnetically conjugate ionospheres, eventually leads to substorm onset; the auroral signatures of breakup occur in the conjugate ionospheres also, dictated by the mapping in the twisted tail.

[21] The onset sector could be the region in which the magnetic field lines are more tail-like, i.e., more stretched, than to either side at earlier and later local times, a possibility also suggested by *Gérard et al.* [2004] and *Donovan et al.* [2008]. This could manifest itself in the growth phase as enhanced auroral emission due to pitch angle scattering in the nondipolar magnetic configuration [e.g., *Sergeev et al.*, 1983]. This stretched field line region would favor the onset of magnetotail plasma instabilities leading to substorm onset. The observations suggest this stretched portion of the tail would be ~2 h of MLT wide.

[22] A final possibility is that the preexisting emission in the growth phase is associated with elevated ionospheric

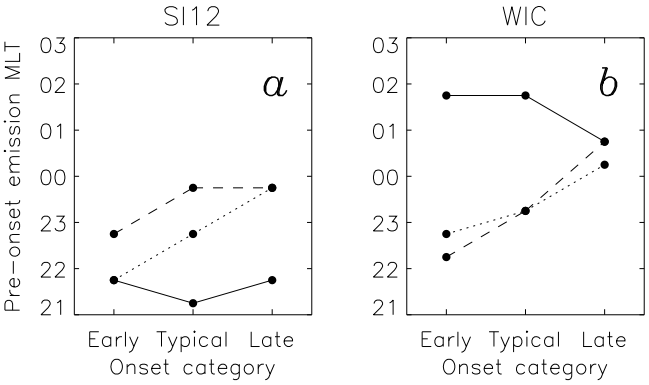


**Figure 7.** The MLT of peak emission during the growth phase of substorms in the categories *a* to *i* for (a) SI12 and (b) WIC. Solid, dotted, and dashed curves correspond to the low, middle, and high onset latitude categories, respectively.

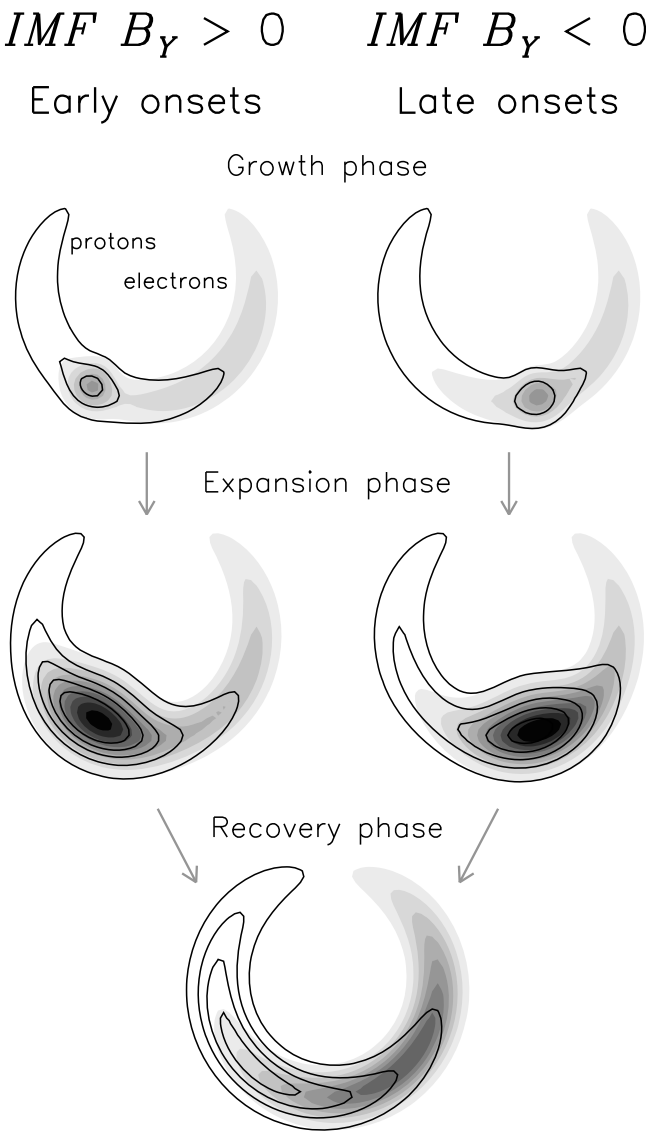


**Figure 8.** Schematic representation of the growth, expansion and recovery phase distributions of electron (gray scale) and proton (contours) aurorae for early (left) and late (right) onset substorms.

conductivities, and this in turn influences magnetosphere-ionosphere coupling favoring this sector for substorm onset.

## 5. Summary

[23] Superposed epoch analysis of the local time distribution of auroral emission associated with substorms of differing onset MLTs reveals a number of things.

[24] 1. For up to an hour prior to onset during the growth phase there is preexisting but faint auroral emission, associated with both precipitating protons and electrons, in the local time sector in which onset subsequently takes place.

[25] 2. During the expansion phase the electron and proton auroral bulge expands eastward and westward roughly symmetrically, such that the bulge remains centered on the onset MLT.

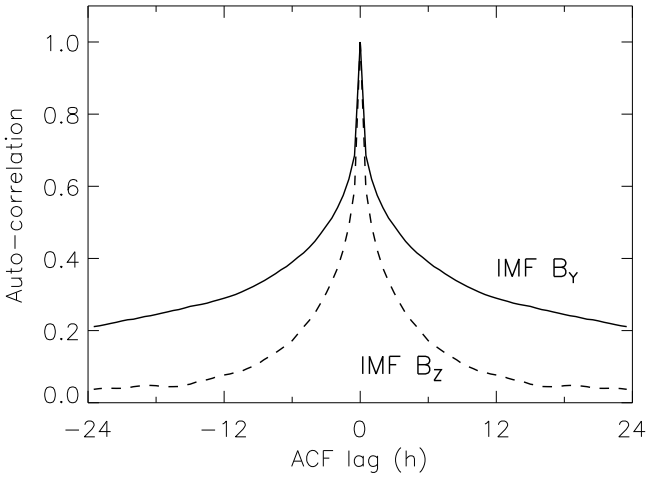


**Figure 9.** Autocorrelation functions of IMF $B_Z$ (dashed curve) and $B_Y$ (solid curve) for 6 years of observation, 2000 to 2005 inclusive.

[26] 3. At 30 min after onset the bulge begins to fade, and as it does so the centroids of proton and electron precipitation move into the premidnight and postmidnight sectors, respectively, as the injected particles drift under the influence of gradient and curvature drift.

[27] 4. The local time sector of onset is determined by the prevailing sense of IMF $B_Y$, such that in the Northern Hemisphere they are located at earlier MLTs for $B_Y > 0$ and later MLTs for $B_Y < 0$. We interpret this as mapping to roughly the central region of the tail, with the local time offset caused by mapping in a twisted magnetotail. A superposed epoch analysis of IMF $B_Y$ keyed to the time of substorm onset suggests that $B_Y$ must have a bias to positive or negative values for several hours to influence the onset MLT. This might be the timescale necessary to produce a significant twist of the magnetotail. Autocorrelation analyses of IMF $B_Y$ and $B_Z$ show that $B_Y$ is less variable than $B_Z$ allowing a magnetotail twist to develop over several hours, perhaps over two or more consecutive growth phases.

[28] **Acknowledgments.** SEM and AG were supported by STFC rolling grant PP/E000983/1. The IMAGE FUV data were supplied by the NASA Space Science Data Centre (NSSDC), and we are grateful to the PI of FUV, S. B. Mende of the University of California at Berkeley, for its use. The ACE data used in this study were accessed through CDAWeb. The authors would like to thank N. F. Ness at the Bartol Research Institute and D. J. McComas of the Southwest Research Institute, for use of the MAG and SWEPAM data, respectively.

[29] Robert Lysak thanks Akira Morioka and another reviewer for their assistance in evaluating this paper.

## References

Akasofu, S.-I. (1964), The development of the auroral substorm, *Planet. Space Sci.*, *12*, 273–282, doi:10.1016/0032-0633(64)90151-5.

Baker, D. N., T. I. Pulkkinen, V. Angelopoulos, W. Baumjohann, and R. L. McPherron (1996), Neutral line model of substorms: Past results and present view, *J. Geophys. Res.*, *101*, 12,975–13,010, doi:10.1029/95JA03753.

Cowley, S. W. H. (1981), Magnetospheric asymmetries associated with the y-component of the IMF, *Planet. Space Sci.*, *29*, 79–96, doi:10.1016/0032-0633(81)90141-0.

Cowley, S. W. H., and M. Lockwood (1992), Excitation and decay of solar wind-driven flows in the magnetosphere-ionosphere system, *Ann. Geophys.*, *10*, 103–115.

Donovan, E., et al. (2008), Simultaneous THEMIS in situ and auroral observations of a small substorm, *Geophys. Res. Lett.*, *35*, L17S18, doi:10.1029/2008GL033794.

Dungey, J. W. (1961), Interplanetary magnetic fields and the auroral zones, *Phys. Rev. Lett.*, *6*, 47–48, doi:10.1103/PhysRevLett.6.47.

Dungey, J. W. (1963), The structure of the exosphere or adventures in velocity space, in *Geophysics, The Earth's Environment*, edited by C. De Witt, J. Hieblot, and L. Le Beau, pp. 503–550, Gordon and Breach, New York.

Frank, L. A., and J. D. Craven (1988), Imaging results from Dynamics Explorer 1, *Rev. Geophys.*, *26*, 249–283, doi:10.1029/RG026i002p00249.

Freeman, M. P., and S. K. Morley (2009), No evidence for externally triggered substorms based superposed epoch analysis of IMF $B_Z$, *Geophys. Res. Lett.*, *36*, L21101, doi:10.1029/2009GL040621.

Frey, H. U., S. B. Mende, V. Angelopoulos, and E. F. Donovan (2004), Substorm onset observations by IMAGE-FUV, *J. Geophys. Res.*, *109*, A10304, doi:10.1029/2004JA010607.

Gérard, J.-C., B. Hubert, A. Grard, M. Meurant, and S. B. Mende (2004), Solar wind control of auroral substorm onset locations observed with the IMAGE-FUV imagers, *J. Geophys. Res.*, *109*, A03208, doi:10.1029/2003JA010129.

Grocott, A., J. A. Wild, S. E. Milan, and T. K. Yeoman (2009), Superposed epoch analysis of the ionospheric convection evolution during substorms: Onset latitude dependence, *Ann. Geophys.*, *27*, 591–600, doi:10.5194/angeo-27-591-2009.

Gussenhoven, M. S., D. A. Hardy, and N. Heinemann (1987), The equatorward boundary of auroral ion precipitation, *J. Geophys. Res.*, *92*, 3273–3283, doi:10.1029/JA092iA04p03273.

Hardy, D. A., M. S. Gussenhoven, and E. Holeman (1985), A statistical-model of auroral electron-precipitation, *J. Geophys. Res.*, *90*, 4229–4248, doi:10.1029/JA090iA05p04229.

Hardy, D. A., M. S. Gussenhoven, and D. Brautigam (1989), A statistical model of auroral ion precipitation, *J. Geophys. Res.*, *94*, 370–392, doi:10.1029/JA094iA01p00370.

Liou, K., C.-I. Meng, and C.-C. Wu (2006), On the interplanetary magnetic field $B_Y$ control of substorm expansion, *J. Geophys. Res.*, *111*, A09312, doi:10.1029/2005JA011556.

Lockwood, M., and S. W. H. Cowley (1992), Ionospheric convection and the substorm cycle, in *Proceedings of the International Conference on Substorms (ICS-1)*, *Eur. Space Agency Spec. Publ., ESP SP-335*, 99–109.

McComas, D. J., S. J. Bame, P. Barker, W. C. Feldman, J. L. Phillips, P. Riley, and J. W. Griffee (1998), Solar Wind Electron Proton Alpha Monitor (SWEPAM) for the Advanced Composition Explorer, *Space Sci. Rev.*, *86*, 563–612, doi:10.1023/A:1005040232597.

Mende, S. B., et al. (2000a), Far ultraviolet imaging from the IMAGE spacecraft. 1. System design, *Space Sci. Rev.*, *91*, 243–270, doi:10.1023/A:1005271728567.

Mende, S. B., et al. (2000b), Far ultraviolet imaging from the IMAGE spacecraft. 2. Wideband FUV imaging, *Space Sci. Rev.*, *91*, 271–285, doi:10.1023/A:1005227915363.

Mende, S. B., H. U. Frey, B. J. Morsony, and T. J. Immel (2003), Statistical behaviour of proton and electron auroras during substorms, *J. Geophys. Res.*, *108*(A9), 1339, doi:10.1029/2002JA009751.

Milan, S. E. (2009), Both solar wind-magnetosphere coupling and ring current intensity control of the size of the auroral oval, *Geophys. Res. Lett.*, *36*, L18101, doi:10.1029/2009GL039997.

Milan, S. E., M. Lester, S. W. H. Cowley, K. Oksavik, M. Brittnacher, R. A. Greenwald, G. Sofko, and J.-P. Villain (2003), Variations in polar cap area during two substorm cycles, *Ann. Geophys.*, *21*, 1121–1140, doi:10.5194/angeo-21-1121-2003.

Milan, S. E., G. Provan, and B. Hubert (2007), Magnetic flux transport in the Dungey cycle: A survey of dayside and nightside reconnection rates, *J. Geophys. Res.*, *112*, A01209, doi:10.1029/2006JA011642.

Milan, S. E., P. D. Boakes, and B. Hubert (2008), Response of the expanding/contracting polar cap to weak and strong solar wind driving: Implications for substorm onset, *J. Geophys. Res.*, *113*, A09215, doi:10.1029/2008JA013340.

Milan, S. E., A. Grocott, C. Forsyth, S. M. Imber, P. D. Boakes, and B. Hubert (2009a), A superposed epoch analysis of auroral evolution during substorm growth, onset and recovery: Open magnetic flux control of substorm intensity, *Ann. Geophys.*, *27*, 659–668, doi:10.5194/angeo-27-659-2009.

Milan, S. E., J. Hutchinson, P. D. Boakes, and B. Hubert (2009b), Influences on the radius of the auroral oval, *Ann. Geophys.*, *27*, 2913–2924, doi:10.5194/angeo-27-2913-2009.

Milan, S. E., T. A. Evans, and B. Hubert (2010), Average auroral configuration parameterized by geomagnetic activity and solar wind conditions, *Ann. Geophys.*, *28*, 1003–1012, doi:10.5194/angeo-28-1003-2010.

Østgaard, N., N. A. Tsyganenko, S. B. Mende, H. U. Frey, T. J. Immel, M. Fillingim, L. A. Frank, and J. B. Sigwarth (2005), Observations and model predictions of substorm auroral asymmetries in the conjugate hemispheres, *Geophys. Res. Lett.*, *32*, L05111, doi:10.1029/2004GL022166.

Østgaard, N., S. B. Mende, H. U. Frey, J. B. Sigwarth, A. Åsnes, and J. M. Weygand (2007), Conjugate imaging of substorms, in *Proceedings of the Eighth International Conference on Substorms* (ICS-8), edited by M. Syrjäsuo and E. Donovan, pp. 215–218, Univ. of Calgary, Alberta, Canada.

Sergeev, V. A., E. M. Sazhina, and N. A. Tsyganenko (1983), Pitch-angle scattering of energetic protons in the magnetotail current sheet as the dominant source of their isotropic precipitation into the nightside ionosphere, *Planet. Space Sci.*, *31*, 1147–1155, doi:10.1016/0032-0633(83)90103-4.

Smith, C. W., J. L'Heureux, N. F. Ness, M. H. Acuña, L. F. Burlaga, and J. Scheifele (1998), The ACE Magnetic Field Experiment, *Space Sci. Rev.*, *86*, 613–632, doi:10.1023/A:1005092216668.

Stone, E. C., A. M. Frandsen, R. A. Mewaldt, E. R. Christian, D. Marglies, J. F. Ormes, and F. Snow (1998), The Advanced Composition Explorer, *Space Sci. Rev.*, *86*, 1–22, doi:10.1023/A:1005082526237.

A. Grocott and S. Milan, Department of Physics and Astronomy, University of Leicester, Leicester LE1 7RH, UK. (steve.milan@ion.le.ac.uk)

B. Hubert, Laboratory of Planetary and Atmospheric Physics, University of Liege, Liege B-4000, Belgium.